Pergamon

Building and Environment, Vol. 33, No. 1, pp. 43–52, 1998

Printed in Great Britain
0360–1323/98 $19.00+0.00

PII: S0360–1323(97)00030–9

A Ventilated Slab Thermal Storage System Model

M. J. REN*
J. A. WRIGHT*

(*Received* 28 *February* 1997)

A simplified dynamic thermal model of a hollow core concrete slab thermal storage system and associated room is described. The model is based on a thermal network that can address the heat exchange between the slab cores and the ventilation air, the thermal storage in the building fabric, and the effect of the heat disturbances on the room. The increase in convective heat transfer at the corners of the ventilation cores is also discussed. For normal cyclic operation, the simulated mass and zone temperatures are both in phase with measured performance data. The model root mean square error between the simulated and measured performance is no more than 0.5°C for the average slab mass temperature and 1.0°C for the zone air temperature. © 1997 *Published by Elsevier Science Ltd.*

INTRODUCTION

The energy crisis of the 1970s started a move towards the design and operation of energy efficient buildings. With half of the U.K.'s primary energy still being consumed in buildings, the need to reduce building energy consumption is now important in order to restrict the emission of environmental pollutants. One approach that reduces energy consumption is to utilize the building fabric as a thermal energy store. In buildings with low thermal loads, the thermal storage in the building fabric can be sufficient to regulate the room thermal environment. For high thermal loads where airconditioning is required, the integration of the building fabric with the airconditioning plant can reduce the peak demand on the plant capacity and improve operational efficiency.

Two approaches that utilize the building fabric as a thermal store are in use. The first is to expose as much of the internal surface of the building fabric as possible, by for instance having no false ceiling. This increases the heat transfer between the building fabric and the room environment. It is an approach which has been shown to be effective in damping peak summer loads [1, 2], but because of the weak coupling between the building mass and room air, the thermal capacity of the mass is under utilized. The coupling between the mass and the air is increased in the second approach, where the ventilation air is passed through the hollow cores of the floor and ceiling slabs, the turbulent air flow thus increasing the convective heat transfer. The extruded hollow core concrete slabs are integrated with the ventilation system by blocking the core ends and cutting connecting holes between the cores to create an extended air path within the slab (Fig. 1). Having passed through the slab, the air can then enter the room directly via a diffuser, or pass through ductwork to enter the room at a low level as part of a displacement ventilation system. Energy savings from the system of between 13% and 70% have been reported, depending on the particular building and the prevailing weather conditions [3, 4]. In addition to the potential energy savings, the perceived comfort levels are often higher during summer due to the radiant cooling effect from the exposed ceiling slab.

In order to maximize energy savings, the ventilation and thermal storage system must be carefully designed and operated. Both the design and control of the system can be investigated using a computer simulation of the system. The requirements of such a simulation are that it should

- correctly model the heat transfer process along the slab air path;
- model the effective heat capacity of the slab mass;
- simulate the influence of all of the major thermal disturbances on the room environment;
- be able to model the effect of different wall constructions and plant operation strategies, so that the optimum design and operation of the system can be investigated.

To date, little research has been directed towards the modelling of hollow core thermal storage systems. A finite element method has been used to model the heat transfer processes in the slab [5], however only the heat transfer through the thickness of the slab was considered. In general, finite element methods are computationally too intensive to allow the modelling of the major thermal disturbances on a building and to enable the investigation of different plant operation strategies. A mathematical model derived from a heat balance on the room environment and hollow core slab has been developed [4]. Two-dimensional heat transfer was considered, through the thickness of the slab and along the airflow path. However, the slab cores were simplified as two parallel plates with

*Department of Civil and Building Engineering, Loughborough University, Loughborough, Leicestershire LE11 3TU, UK.

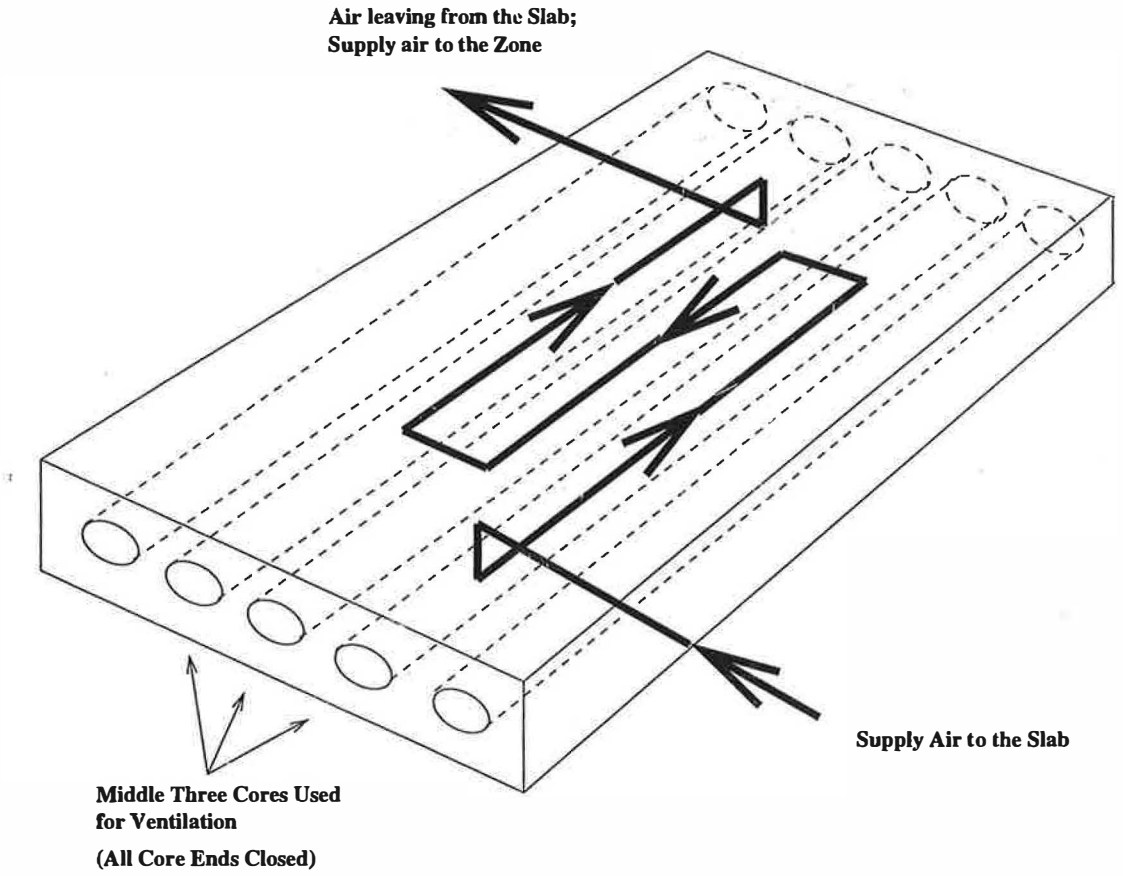

Fig. 1. A hollow core ventilated slab.

air passing between them. A constant heat transfer coefficient along the air path was assumed so that the effect on the heat transfer coefficient of the air flow around the corners of the air path was not modelled. In contrast, computational fluid dynamic modelling methods have been used to study the heat transfer within hollow cores [6]. It was concluded that the majority of the heat transfer takes place at the corners of the air path. The applicability of the computational fluid dynamic modelling approach is limited in that constant boundary conditions are normally assumed, so that the effect of time variant disturbances on the room and slab are not modelled.

To summarize, the existing models are either limited in their modelling of the heat transfer along the slab air path or are unable to represent the effect of time variant disturbances on the room and ventilated slab. This paper presents a thermal network model that addresses these deficiencies.

Lumped parameter thermal network models

The thermal modelling of buildings has been the subject of much research [7] and, as such, the approach adopted in this work is to integrate a new model of the ventilated hollow core slab with an established zone model. The lumped parameter method has been chosen to model the thermal performance of the building zone and ventilated slab. The approach is attractive in that the model parameters are easily derived from the thermal properties of the building materials and that the model equations are easily solved so that parametric studies can be conducted without excessive computation.

An established algorithm has been selected to calculate the model parameters [8, 9]. The algorithm uses the thermal time constants of a building element to obtain the thermal resistances. The algorithm is easily interpreted and can be obtained from a transfer function derivation for a building element. Consider the multi-layer construction shown in Fig. 2 and the lumped parameter representation given in Fig. 3. Here, R_i and R_o are the resistances of the mass node to the disturbances from the inside and outside respectively. C is the total heat capacity of the construction. The time constants, $\tau_i = R_iC$ and $\tau_o = R_oC$, represent the response to a disturbance from inside and outside, and can be calculated thus:

$$\tau_i = \sum_{k=1}^{n} C_k \left(R_{si} + \sum_{j=1}^{k-1} R_j + \frac{R_k}{2} \right) \quad (1)$$

$$\tau_o = \sum_{k=1}^{n} C_k \left(\frac{R_k}{2} + \sum_{j=k+1}^{n} R_j + R_{so} \right), \quad (2)$$

where R_j and R_k are the thermal resistances of layers j and k, and R_{si} and R_{so} are the resistances of the inside and outside surfaces. Having calculated the time constants and the total thermal capacitance of the construction ($C = \sum_{k=1}^{n} C_k$), the lumped thermal resistances can be obtained as $R_i = \frac{\tau_i}{C}$ and $R_o = \frac{\tau_o}{C}$.

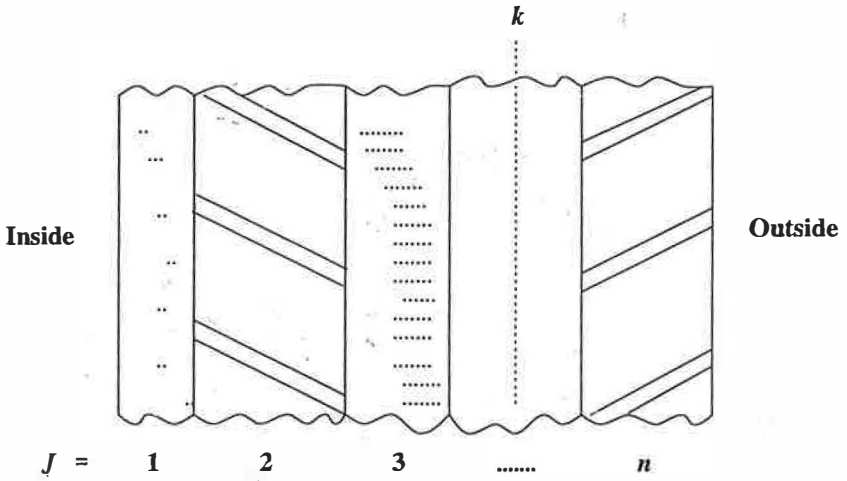

Fig. 2. Multi-layer building element.

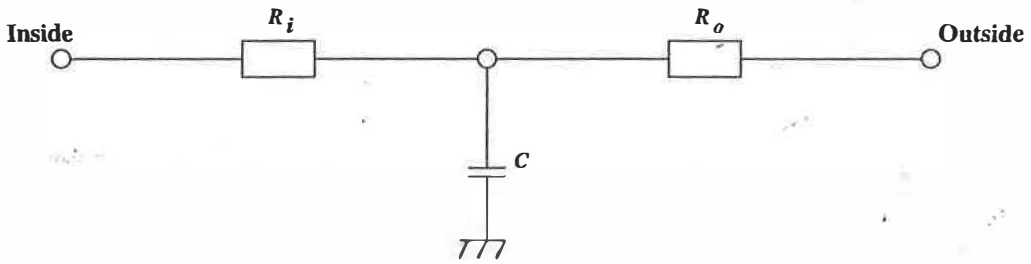

Fig. 3. Lumped parameter model of a building element.

THE VENTILATED SLAB THERMAL MODEL

Previous research [5] suggests that there is a negligible change in the slab concrete mass temperature along the air path. However, since there can be a difference in temperature from one zone to another, the mass temperature may not be distributed symmetrically about the centre of the slab. This effect is accounted for by modelling the slab in two halves, one half coupled to the environment above the slab and the second to the environment below. In order to simplify the model, however, the heat conduction through the concrete slab from one surface to the other is not modelled. This can be justified in that the temperature difference that most affects the slab mass temperature is the difference between the ventilation air temperature and that of the adjacent environment, the temperature difference across the slab having the least effect on the mass temperature. A substantial change in air temperature will exist along the air path, yet a single air temperature is required for the ventilation air node in the lumped parameter model. This has been taken as the average air temperature along the air path which can be derived from the heat exchange between the slab and the ventilation air.

The lumped parameter model of the ventilated slab is illustrated in Fig. 4. $\bar{T}_{av}$ is the mean temperature of the ventilation air, and T_{au} and T_{al} are the air temperatures of the zones above and below the slab. R_{cu} and R_{cl} are the slab thermal resistances of the mass nodes to disturbances in the zone air temperatures. R_{cu} and R_{cl} are not equal due to the different floor and ceiling finishes. Similarly the thermal capacitance, C_u and C_l, of the two halves of the slab can differ due to the surface finishes. Although the surface resistance and the resistance of the concrete between the mass node and the ventilation air are the same for both sides of the slab, the procedure for deriving the resistances from the time constants means that the finishes on the external surfaces will also result in R_{au} and R_{al} being different.

Ventilation air to slab heat exchanger model

Since the slab mass temperature is constant along the air path, the heat exchange between the ventilation air and the slab is in effect that of a heat exchanger with one fluid condensing or evaporating and therefore being of infinite thermal capacity. If the slab mass temperature is taken as the arithmetic mean, $\bar{T}_m$, of the two slab mass temperatures T_{mu} and T_{ml} (Fig. 4), then the air temperature at a distance x along the airpath is given by

$$T_{ax} = \bar{T}_m + (T_{ai} - \bar{T}_m)e^{-\alpha x}. \quad (3)$$

αx is the number of transfer units and

$$\alpha = \frac{U}{\dot{m}_a c_{pa}}.$$

$\dot{m}_a$ is the air mass flow rate and c_{pa} the air specific heat capacity. U is the transmittance per unit length of the airpath derived from the resistances R_{au} and R_{al} (Fig. 4). T_{ai} is the temperature of the air at inlet to the slab. The average air temperature along the airpath $\bar{T}_{av}$ can be obtained by integrating T_{ax} along the length of airpath L

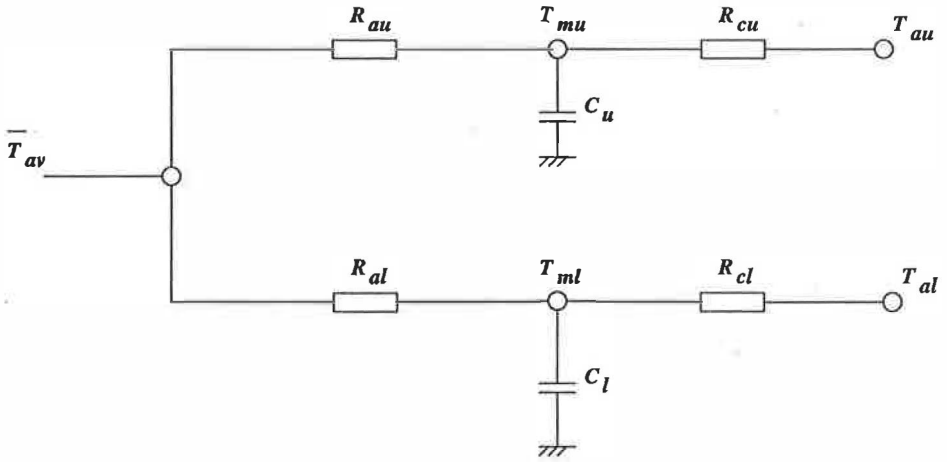

Fig. 4. Lumped parameter model of the ventilated slab.

$$T_{av} = \frac{\int_0^L T_{ax}\,dx}{L}.$$

$$\bar{T}_{av} = \bar{T}_m + \frac{(T_{ai} - \bar{T}_m)}{\alpha L}(1 - e^{-\alpha L}). \quad (4)$$

The slab thermal capacitance

A typical concrete slab will have five cores but only three are generally used for ventilation. This, and the air path taken through the slab (Fig. 1), makes it difficult to determine the effective thermal capacitance of the slab. Previous research [6] suggested that a 24-hour cyclic variation of the surface temperature of a slab influences the mass to a depth of only 15.0 cm. However, using this depth to determine the thermal capacitance has proved to be ineffective when used in the model described here. The approach adopted to determining the slab thermal capacitance is first to simplify the representation of the air paths [6] (Fig. 5), and second select a width and length of slab to provide a capacitance that gives a thermal response that matches measured performance data from a commercially available system. The total length of the simplified air path is equal to that of the real system. The width of the area relating to the effective thermal capacitance W has been set to equal the span of hollow core section of the slab (Fig. 6). In order to match the measured thermal performance of a commercial ventilated slab system, the length of slab beyond the core ends Δ (Fig. 5) was found to be 30.0 cm. The remainder of the slab length and the area of slab beyond W is integrated into the building zone mass node.

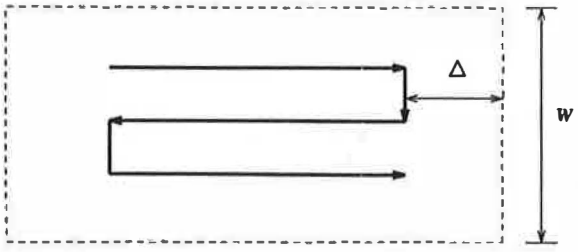

Fig. 5. Simplified air path and area of thermal capacitance.

The slab concrete thermal resistances

Due to the geometry of the slab, the calculation of the slab concrete resistance is considered in two parts. When calculating the resistance to a disturbance in the room air temperature, the slab is considered as a flat plate with a cross-sectional area equal to the effective storage area of the slab. The thickness of the plate used to assess the resistance is then $\delta = A/Z$ (Fig. 6). However, radial heat transfer occurs between the ventilation air and the slab. Since, for most commercial systems, the distance between the cores is similar to the thickness of slab above and below the cores, the mass node is assumed to be located close to the perimeter of a circle positioned half way between the edge of the core and the external surface of the slab (Fig. 6). The circle is centered on the core and is of diameter D. Here, an isothermal cylinder has been assumed such that the resistance R_c for half the core is given by

$$R_c = \frac{\ln\left(\frac{D}{d}\right)}{\pi K L}, \quad (5)$$

where K is the conductivity of the concrete. As for all lumped parameter resistances, the relationship may not be true for highly transient stages of heat transfer. It is also unlikely that true isothermal conditions will occur on the edge of the cylinder. However, this is unlikely to significantly affect the accuracy of the lumped parameter model.

The ventilation air surface resistance

The resistance on the inside surface of the air cores, R_{sa}, is derived from the surface heat transfer coefficient. This is a function of the properties of both the air flow and the nature of the surface of the cores. The heat transfer is also higher around the connecting corners than along the straight sections of core. To further complicate the calculation of the surface resistance, the model must allow for a variable air flow rate.

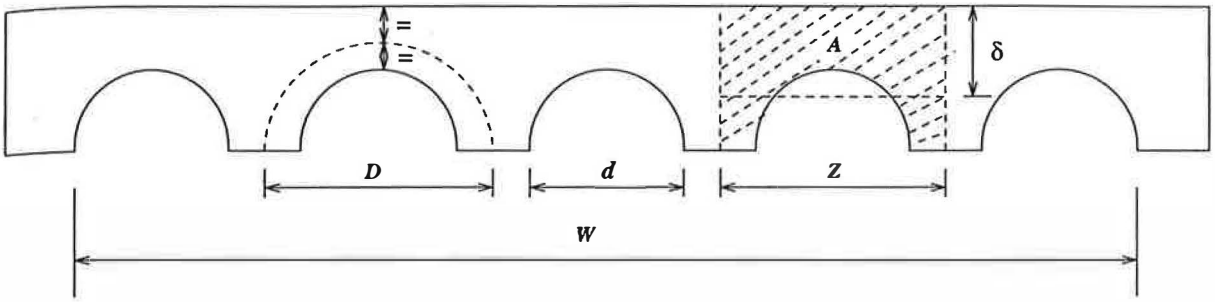

Fig. 6. Dimensions for slab concrete capacitance and resistance calculations.

Since no reliable measurements have been made of the heat transfer coefficient inside hollow core slabs, the approach adopted here is to use a standard heat transfer correlation for the resistance of the straight sections of the core, and to correct this for the enhanced heat flow around the corners, the correction factor having been obtained from the measured performance of a commercial ventilated slab system. The empirical correlation for the straight cores has been taken as [10, 11]

$$\mathrm{Nu} = 0.023\mathrm{Re}^{0.8}\mathrm{Pr}^{0.4}, \tag{6}$$

where Nu is the Nusselt number, Re the Reynolds number and Pr the Prandtl number. Using the properties of air at a temperature of 20.0°C, the heat transfer coefficient h_{sa} for the straight section of duct can then be given by the approximate expression

$$h_{sa} = 3.73v^{0.8}d^{-0.2}\,(\mathrm{W/m^2\,K}), \tag{7}$$

where v is the air velocity and d the core diameter.

Measured air temperatures from a commercially available ventilated slab system suggest that this relationship is of the correct order. The accuracy of this relationship could not be verified completely since the data available are insufficient to enable precise in the measurement of the heat transfer coefficients. Air temperatures measured along the air path suggest that the heat transfer coefficient for the corners is of the order of 50 times higher than that for the straight sections of core. This was determined using the measured data and the heat exchanger model. The value was further verified by comparing the lumped parameter model output to a range of measured performance data. The consistency of the increase in corner heat transfer with velocity has not been verified completely, since measured data was only available for two core air velocities. It is unlikely, however, that the relationship between straight core and corner heat transfer will change significantly provided the velocity remains in the fully turbulent region.

THE LUMPED PARAMETER ZONE MODEL

Lumped parameter models and the thermal network approach have been the subject of much research [8, 12–15]. The model adopted as the basis of this work gives a clear insight into the thermal performance of the building and has been validated for a wide range of building types [9, 16–18].

The model is illustrated in Fig. 7, where T_{sa} is the sol-air temperature, T_o the outside air temperature, and T_{az} the zone air temperature. T_{sb} and T_{mb} represent the zone inside surface and mass temperatures. Q_c and Q_r are the convective and radiant heat gains. R_{sb} is the convective heat transfer resistance and R_v the infiltration resistance.

C_b is the effective thermal capacitance of all massive elements in the zone. R_{ob} and R_{ib} are obtained by combining, in parallel, the internal and external resistances of all massive elements of the building fabric. Windows are considered to have no thermal capacity but their resistance is integrated in R_{ob} and R_{ib}. The internal partitions are also lumped into R_{ob}, R_{ib} and C_b. This is achieved by representing the temperature of the adjoining zones by the dry resultant temperature and using this in the same manner as the sol-air temperature used for the external walls.

The shortwave radiation on the exposed external surfaces is modelled by the sol-air temperature T_{sa}. T_{sa} is calculated according to the convective and radiant heat transfer occurring on the external surfaces. As the surfaces are at different orientations they will receive a

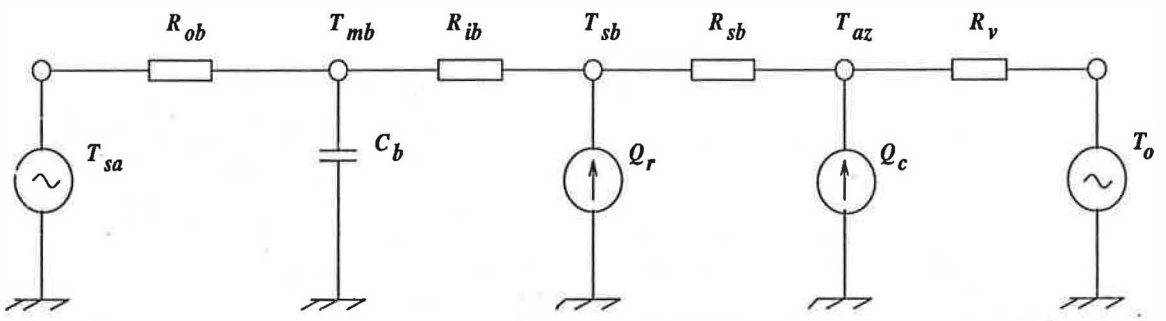

Fig. 7. Lumped parameter first-order building model.

different amount of solar radiation (or heat disturbances from the adjoining zones). T_{so} is therefore corrected for all walls based on the fact that walls are in parallel from the indoor air node to outside air node (or adjoining zone air node) [9].

$$T_{sa} = \sum_{k=1}^{n} T_{sa,k} \frac{R_{\text{total}}}{R_k}, \tag{8}$$

where R_k is the total resistance for one element between the inside air and outside air node and R_{total} is the sum of R_k in parallel.

THE COMBINED THERMAL NETWORK MODEL FOR BUILDING ZONE AND SLAB

The lumped parameter building model has been extended to incorporate two ventilated hollow core slabs, one for the ceiling and a second for the floor. Since the room surfaces may be at noticeably different temperatures when the ventilated hollow core slabs are in use, the longwave radiant heat exchange between the room surfaces has been modelled. The new model also includes the shortwave radiant heat gain distribution to the different surfaces of the room.

Figure 8 represents the thermal network for the integrated ventilated slab and building model. The notation is as described for Figs 4 and 7, except for the modelling of the heat exchange between surfaces and in order to allow for two ventilated slabs (subscripts c and f have been added to denote the ceiling and floor). Unlike for Fig. 4, R_{cic} and R_{cuf} are the conductive resistances from the ceiling and floor slab mass nodes to the internal surfaces of the zone; the surface resistances (R_{sc}, R_{sf}) are represented separately to allow the modelling of radiant heat exchange between the surfaces.

The mass temperatures have been omitted for clarity whereas the internal surface temperatures for the walls, ceiling and floor are T_{sw}, T_{sc} and T_{sf} respectively. $\hat{T}_{avc}$ and $\hat{T}_{avf}$ are mean ventilation air temperatures for the ceiling and floor slabs. T_{ac} and T_{af} are the temperatures of the zones above the ceiling and below the floor. T_{az} is the air temperature of the modelled zone which is coupled to the wall, ceiling and floor surfaces by the convective surface resistances R_{sb}, R_{sc} and R_{sf}.

C_a represents zone air thermal capacitance, however the effect of the room air capacity on the building response is insignificant compared with the effect due to the structural elements. Further, the high frequency response is only a minor consideration in this study and therefore the air capacitance is not normally included in the model. The convective heat gain, Q_c, includes the heat gain from the ventilation system supplied via the ceiling slab.

The equations resulting from the model have been solved in this study using a state–space representation and the Runge–Kutta numerical integration method.

Longwave radiant heat exchange

The long wave radiant heat exchange between surfaces is modelled by the exchange with the radiant star index temperature T_{rs}. This temperature is coupled to the room surfaces by the radiant resistance R_{rw} for the walls, R_{rc} for the ceiling and R_{rf} for the floor. The radiant star temperature is represented by [19]

$$T_{rs} = \frac{S_w T_{sw} + S_c T_{sc} + S_f T_{sf} + Q_{lr}}{S_w + S_c + S_f}, \tag{9}$$

where Q_{lr} is the longwave radiant heat gain generated from equipment, lighting and occupancy. T_{sw}, T_{sc} and T_{sf} are the surface temperatures of the walls, ceiling and floor. S_w, S_c and S_f are radiant conductances for the walls, ceiling and floor. They depend on the surface area, emissivity and radiant heat transfer coefficient associated with each element. For example, for the ceiling

$$S_c = A_c E_c h_r,$$

where A_c is ceiling surface area, h_r is the radiant heat transfer coefficient of the room and E_c a function of emissivity. h_r is a function of T_{rs}^3 and so, in order to avoid iteration, T_{rs} is assumed to be 20°C when calculating h_r [19]. E_c can be calculated from [19]

$$\frac{1}{E_c} = \frac{1-\epsilon_c}{\epsilon_c} + \gamma_c, \tag{11}$$

where ϵ_c is the ceiling surface emissivity. γ_c is the ceiling area weighting factor, $\gamma_c = 1-(A_c/A_{\text{total}})$, where A_{total} is the sum of the areas of the walls, ceiling and floor.

The same algorithms are equally applicable to S_w and S_f. Inversion of the conductances gives the radiant resistances R_{rw}, R_{rc} and R_{rf}.

Shortwave heat gain

Q_r is the shortwave heat gain to the zone. The shortwave gain transmitted through the windows is calculated hour by hour from the weather data. The proportion of incoming radiation distributed onto the wall surfaces, ceiling surface and floor surface, is calculated according to the relative surface areas. The total gain absorbed by each element is the product of shortwave radiant surface coefficient, the proportion of radiation distributed to the surface, and the total shortwave gain entering the room.

Model initialization

During the comparison of the model accuracy with measured performance data, the model was initialized using the measured data values. More generally, if a uniform temperature is assumed as the initial condition for all the mass elements of the zone, then executing the model for four days of identical weather data has been shown to be sufficient to eliminate the effects of this assumption. Similarly, any improvement in accuracy due to the numerical integration has been shown to be insignificant for integration times shorter than 20 minutes.

MODEL PREDICTION AND COMPARISON WITH MEASURED DATA

The output from the ventilated slab and zone model has been compared with measured data from an experimental test facility. The test room is 4.80 m × 4.00 m × 3.75 m with a door but no window. The walls are of a light weight, being simply constructed and insulated with expanded polystyrene slabs. The floor and ceiling are constructed from four commercially available hollow core concrete slabs. Only the ceiling is used as a

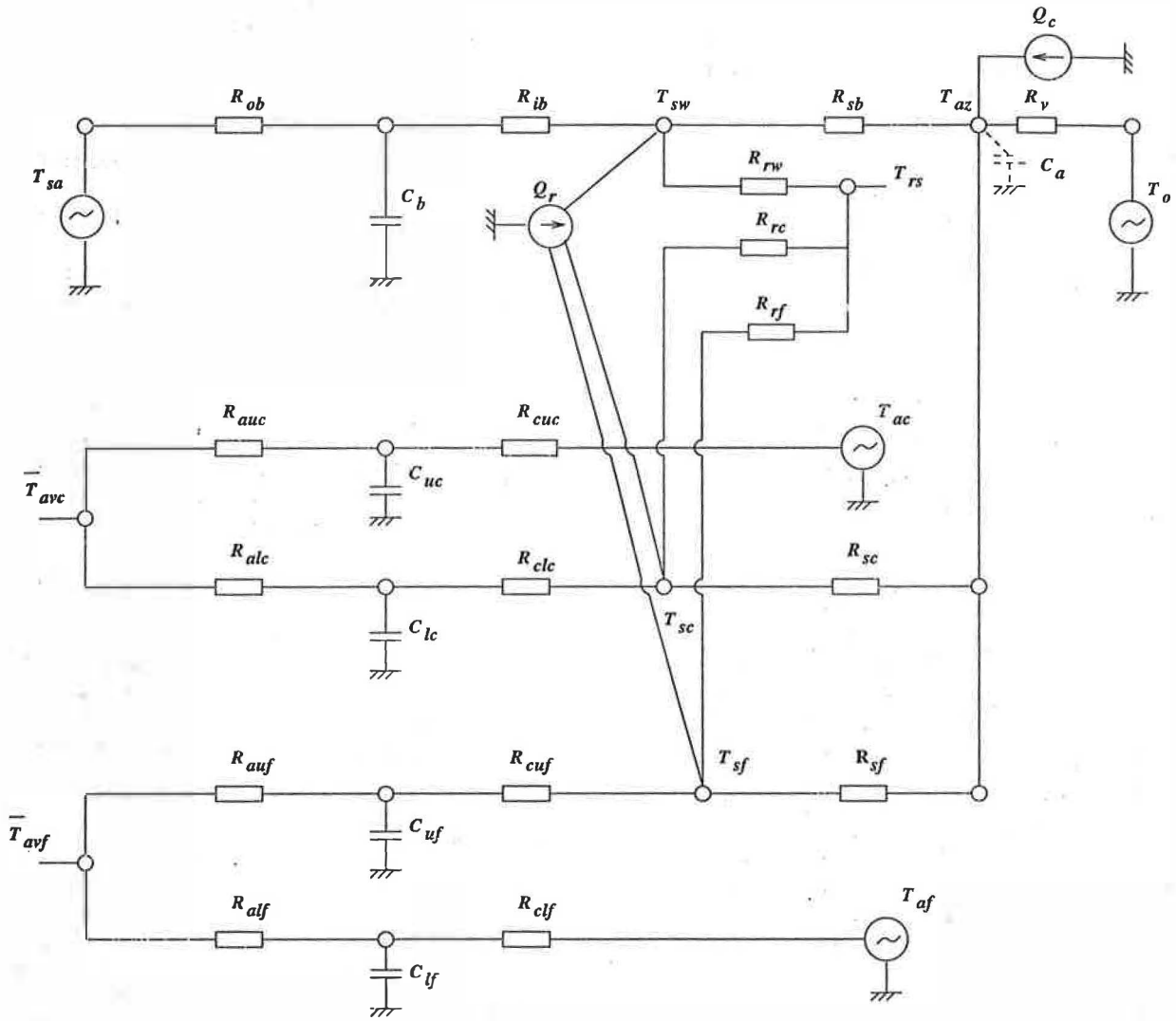

Fig. 8. Combined building and ventilated slab model.

ventilated slab system with the middle two out of the four slabs being modified to provide ventilation ducts. The ceiling also has a 35.0 mm screed covering the upper surface.

The test room is located in a large laboratory hall and therefore the test room's external environment is that of the test hall. The ventilated slab system and room is supplied with the air from a central air handling unit which maintains a preset air mass flow rate and temperature. In the tests, the same proportion of air from the plant was supplied equally to both ceiling slabs. The air from the two slabs was then combined and delivered to the room. The lightweight construction of the test room and the absence of any windows are an advantage in evaluating the performance of the model, since the new aspects of the model are concerned with the ventilated slab system, the zone model being well established.

The room temperature was measured by a sensor positioned in the middle of the test room. Velocity and temperature measurements were made inside the ventilated slab cores and the slab mass temperature was measured at two depths, 70.0 and 210.0 mm from the upper surface (the slabs being 270.0 mm thick with 180.0 mm core diameter). The overall average mass temperature has been taken as the mean of the measurements at both depths.

The model output has been compared to two sets of test data. The first set is for normal cyclic operation, at two air velocities, 1.18 m/s ($Re = 1.4 \times 10^4$) and 3.75 m/s ($Re = 4.48 \times 10^4$). The second set is for a step change in air flow temperature supplied to the slab at an air velocity of 1.05 m/s.

In order to quantify the differences between the predicted results and the measured data, three standard error functions have been adopted, the maximum absolute error (e_{max}), the maximum percentage error (e_{pct}), and the root mean square error (e_{rms}). The maximum absolute error between the predicted and measured data is useful in a comparison with the accuracy that could be expected from industrial standard sensors. The maximum error expressed as a percentage of the measured values indicates the relative accuracy of the model. The root mean square error indicates the average accuracy over the whole simulation time period, although this error is sensitive to extreme errors.

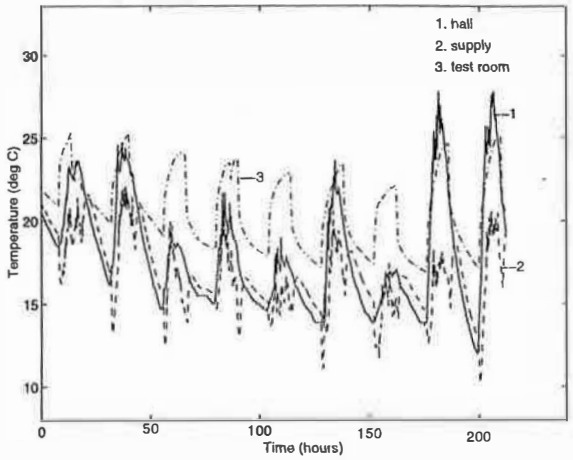

Fig. 9. Test measurements (1.18 m/s velocity).

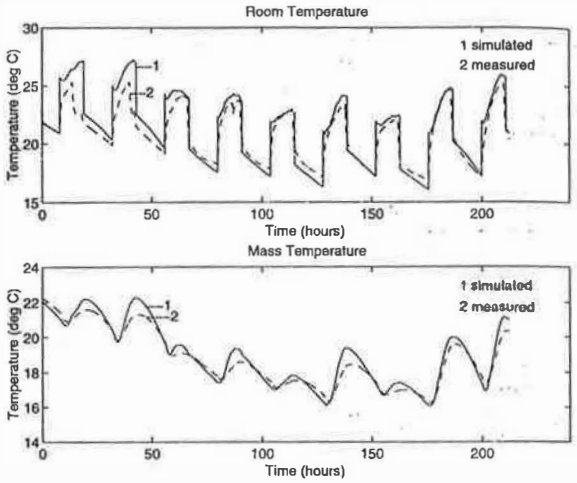

Fig. 11. Measured and simulated performance (1.18 m/s velocity).

Model accuracy for cyclic operation

The cyclic tests emulate normal daily operation of the ventilated slab system. During these tests, the room heat gains were imitated by a convector heater of approximately 1.0 kW output. Both the heater and ventilation air supply were in operation between 8:00 am and 7:00 pm. During the other periods, there was no ventilation and no room heat gain.

Figure 9 shows the measured temperatures for an air velocity of 1.18 m/s in the slab core. The *hall* temperature is the test room's external air temperature and the *supply* temperature is that of the air entering the ventilated slab. Figure 10 illustrates the same variables but for a supply air velocity of 3.75 m/s in the slab cores.

Figure 11 compares the model output with the measured data for an air velocity of 1.18 m/s. The predicted and measured results are in phase but an error in peak amplitude of approximately 1.0°C in the room air temperature is apparent during the period of heat gain and ventilation. This error can be partly attributed to the uncertainty in the output of the convector heater during this test period. Similarly, Fig. 12 shows the simulated and measured data for an air velocity of 3.75 m/s in the air cores. For both tests, the mass temperatures suggest that the simulated model is more responsive than the test slab. Since the thermal capacity and density of the concrete have been measured, the faster response of the model can be attributed to the uncertainties in the calculation of the thermal resistances and the choice of effective thermal storage volume.

Table 1 gives the errors between the model output and measured data for the zone air temperature $\bar{T}_{az}$, and the average mass temperature $\bar{T}_m$. The maximum errors (e_{max}, e_{prt}) in zone temperature occur during the highly transient periods at the beginning and end of plant operation. However, a maximum root mean square error, e_{rms}, of 1.0°C for the zone air temperature and of 0.5°C for the mass temperature can be considered to be acceptable.

Model accuracy for step input operation

The step input test emulates a winter operation of the system in which, some time prior to the start of occupancy, a step increase is made to the air temperature supplied to the ventilated slab. In this case, the initial supply temperature was set to 12.7°C. At 2:25 pm the

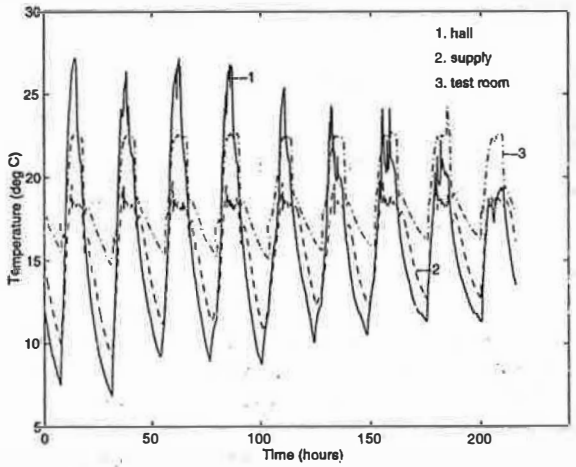

Fig. 10. Test measurements (3.75 m/s velocity).

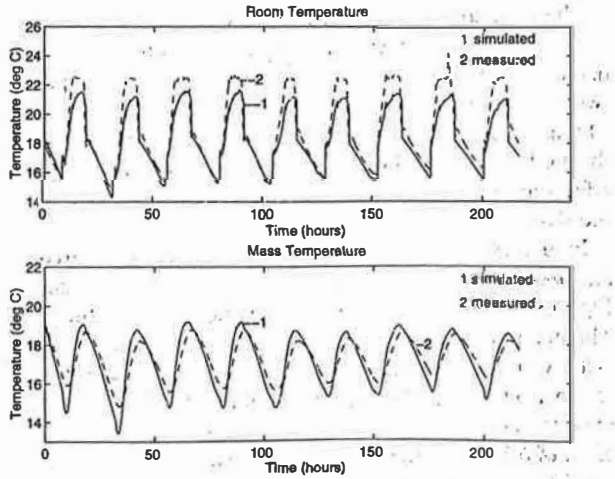

Fig. 12. Measured and simulated performance (3.75 m/s velocity).

Table 1. Model accuracy for cyclic operation

	1.18 m/s		3.75m/s	
Error	$\hat{T}_{az}$	$\hat{T}_{m}$	$\hat{T}_{az}$	$\hat{T}_{m}$
e_{max}	4.2°C	0.7°C	2.3°C	0.9°C
e_{pct}	24.0%	3.6%	12.0%	5.0%
e_{rms}	0.9°C	0.4°C	1.0°C	0.5°C

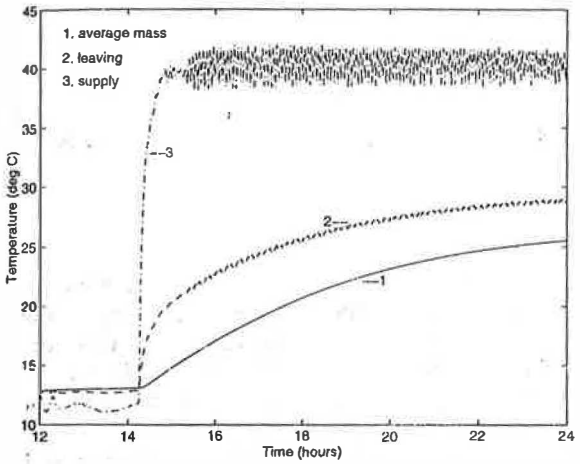

Fig. 13. Step test temperature measurements.

supply air temperature setpoint was increased to 40.0°C. The air velocity in the slab cores was maintained at approximately 1.05 m/s throughout the test. Figure 13 illustrates the measured performance data, in which *supply* is the temperature of the air entering the ventilated slab, *leaving* is the temperature of the air leaving the slab and entering the zone, and finally *mass* is the average mass temperature of the slab. The noise on the supply air temperature is due to the operation of the heating coil control system. The effect of the slab mass on damping the oscillations is apparent from the air temperature leaving the slab.

The zone and hall temperatures were not measured. Therefore the sol-air temperature for the simulation was assumed to be a constant 20.0°C from 8:00 am to 7:00 pm (working hours), and 12.0°C during the other periods. This assumption should not invalidate the comparison of the model output and measured data, since the dominant effects are clearly due to the supply air temperature to the slab.

Figure 14 gives a comparison between the measured and modelled air temperature leaving the slab, whereas Fig. 15 compares the slab mass average temperatures. The maximum error in air temperature leaving the slab is 1.1°C and a root mean square error of 0.6°C over the test period (Table 2). The maximum error in average mass temperature is only 0.3°C with a root mean square error of 0.2°C over the test period. The model is therefore considered to be of an acceptable accuracy by the authors.

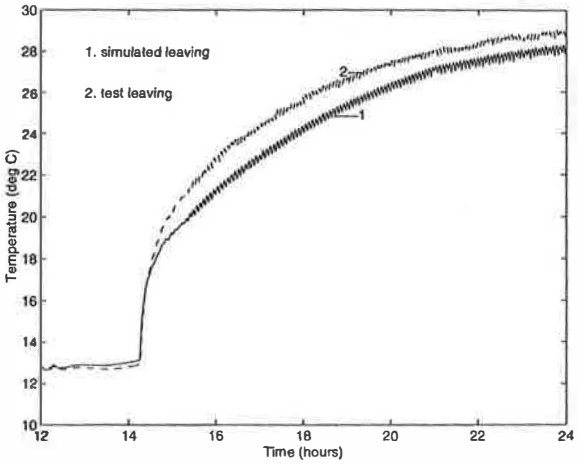

Fig. 14. Step test measured and simulated air leaving temperature.

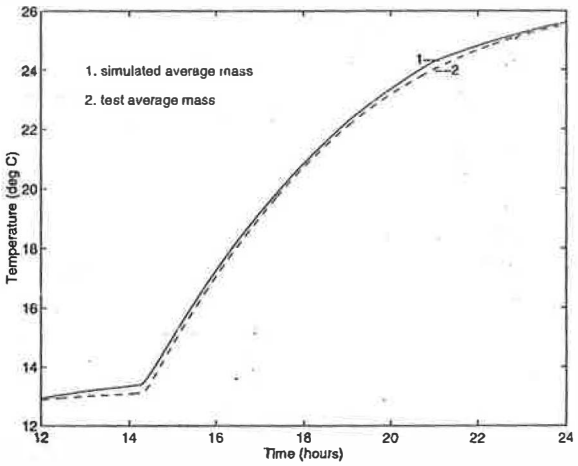

Fig. 15. Step test measured and simulated mass temperature.

Table 2. Model accuracy for step input operation

Error	$\hat{T}_{al}$	$\hat{T}_{m}$
e_{max}	1.1°C	0.3°C
e_{pct}	4.8%	2.5%
e_{rms}	0.6°C	0.2°C

CONCLUSIONS

This paper describes a lumped parameter model of a hollow core concrete slab thermal storage system and associated zone. The integrated slab and zone model includes an established lumped parameter building model. A new model has been developed for the ventilated floor and ceiling slabs, which includes the heat exchange between the ventilation air and the slab. The model parameters are easily obtained and the model equations are easily solved, which will allow the investigation of different design solutions and ventilation plant operating strategies.

In association with the development of the slab heat exchanger model, an analysis of measured performance

data would suggest that the increase in convective heat transfer coefficient around the corners of the air cores is approximately 50 times higher than that for a plain duct. The generality of this value cannot be verified but it appears to be correct for use in the model described in this paper.

The model has been compared to measured performance data for two sets of tests, the first representing normal operation cycled over several days, and the second a step input in the supply air temperature to the slab. It can be concluded that the model gave an acceptable accuracy for normal operation with a root mean square error in zone air temperature of less than 0.9°C. However, a maximum error of 4.2°C in zone air temperature occurred during the highly transient, but brief, period at the beginning of plant operation. The errors are generally due to the amplitude rather than a phase shift in the temperature cycle. The step input test gives an insight into the accuracy of the model of the heat exchange between the ventilation air and the slab. The maximum error in air temperature leaving the ventilated slab was 1.1°C, whereas the maximum error for the average temperature of the slab was 0.3°C, both of which indicate an acceptable level of accuracy.

Acknowledgements—The authors would like to acknowledge the U.K. Building Research Establishment for providing the ventilated slab system measured performance data.

REFERENCES

1. Ruud, M. D., Mitchell, J. W. and A Klein, S., Use of building thermal mass to offset cooling loads. *ASHRAE Transactions*, 1990, **96(2)**, 820–829.
2. Snyder, M. E. and Newell, T. A., Cooling cost minimization using building mass for thermal storage. *ASHRAE Transactions*, 1990, **96(2)**, 830–838.
3. Allen, G., Kani, M. and St. Carpenter, A., Mechanically enhanced passive solar thermal storage. In *Proceedings SESCI* 1984, Calgary, August 1984.
4. Zmeureanu, R. and Fazio, P., Thermal performance of a hollow core concrete floor system for passive cooling. *Building and Environment*, 1988, **23(3)**, 243–252.
5. Angenbroe, G. L. M. and Vedder, H. A., Accurate modelling of air-supplied heat storage in hollow core slabs. *CIMA* 2000, *World Congress on Heating, Ventilation and Air Conditioning*, August 1985, pp. 441–446.
6. Winwood, R., Benstead, R., Edwards, R. and Letherman, K. M., Building fabric thermal storage: use of computational fluid dynamics for modelling. *Building Services Engineering Research and Technology*, 1994, **15(3)**, 171–178.
7. Clarke, J. A., *Energy Simulation in Building Design*. Adam Hilger, Bristol, 1985.
8. Hassid, S., A linear model for passive solar calculations: evaluation of performance. *Building and Environment*, 1985, **20(1)**, 53–59.
9. Mathew, E. H., Richards, P. G. and Lombard, C., A tool for predicting hourly air temperatures and sensible energy loads in buildings at sketch design stage. *Energy and Buildings*, 1989, **14**, 61–80
10. Holman, J. P., *Heat Transfer*. McGraw-Hill, New York, 1986.
11. CIBSE, *Guide Book C3*. The Chartered Institution of Building Services Engineers, London, 1986.
12. Givoni, B., *Man, Climate and Architecture*, 2nd edn. Applied Science, London, 1976, pp. 414–450.
13. Hoffman, M. and Feldman, M., Calculation of the thermal response of buildings by the total thermal time constant method. *Building and Environment*, 1981, **16(2)**, 71–85.
14. Laret, L., Use of general models with a small number of parameters: theoretical analysis. *Proceedings of CLIMA* 2000, Budapest, 1980.
15. Crabb, J. A., Murdoch, N. and Penman, J. M., A simplified thermal response model. *Building Services Engineering Research and Technology*, 1987, **8**, 13–19.
16. Mathew, E. H., Rousseau, P. G. and Richards, P. G., A procedure to estimate the effective heat storage capability of a building. *Building and Environment*, 1991, **26**, 179–188.
17. Lombard, C. and Mathew, E. H., Efficient, steady state solution of a time variable RC network for building thermal analysis. *Building and Environment*, 1992, **27(3)**, 279–287.
18. Mathew, E. H., Richards, P. G. and Lombard, C., A first-order thermal model for building design. *Energy and Buildings*, 1994, **21**, 123–145.
19. Davies, M. G., Definitions of room temperature. *Building and Environment*, 1993, **28(4)**, 383–398.